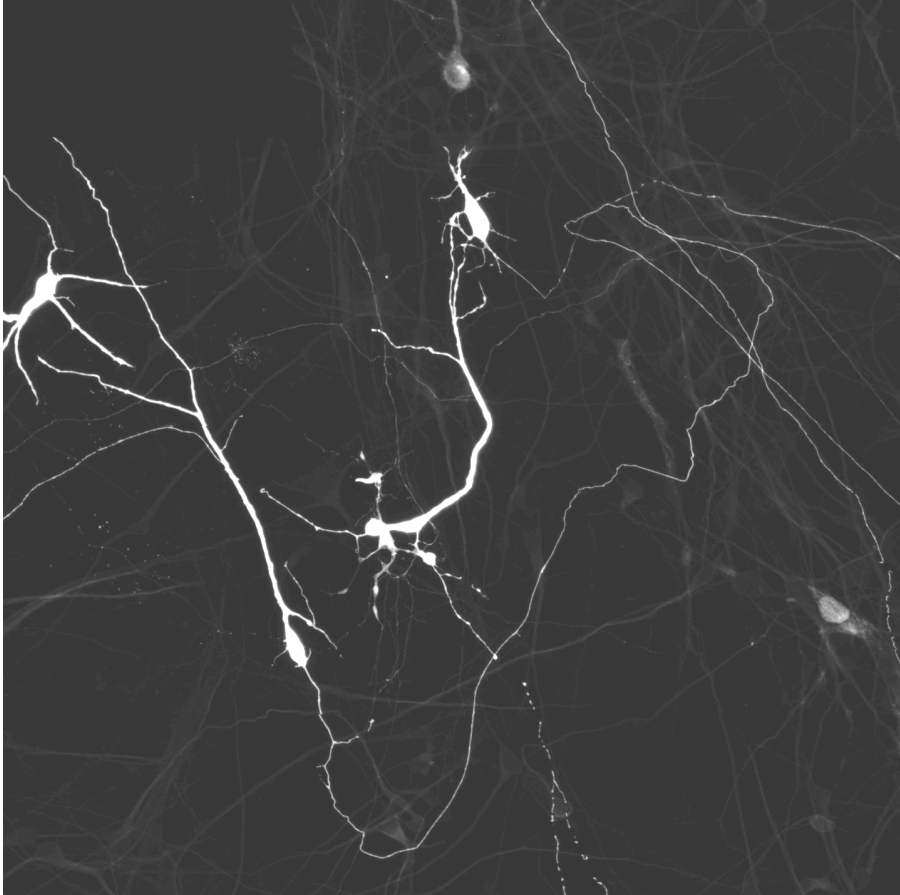


IMAGE ANALYSIS FOR ALL-OPTICAL ELECTROPHYSIOLOGY



by

Polina KOSTINA

in partial fulfillment of the requirements for the degree of
Bachelor of Science
in Nanobiology

at Delft University of Technology,
to be defended publicly on July 1, 2022, at 9:00 am

Supervisors:

Dr. D. Brinks
X. Meng

Thesis committee:

Dr. D. Brinks Delft University of Technology
Dr. E.C.M. Carroll Delft University of Technology

Cover image: Kushner lab, Erasmus MC

An electronic version of this thesis is available at
<http://repository.tudelft.nl/>.



Say what you know, do what you must, come what may.

Sofia Vasilyevna Kovalevskaya, 1889

CONTENTS

Abstract	vii
1 Introduction	1
2 Theory	3
2.1 Cell model	3
2.1.1 Neurons	3
2.1.2 Neuron progenitor cells	6
2.1.3 Spiking HEK cells	8
2.2 All-optical electrophysiology	8
2.2.1 Optopatch	8
2.2.2 Voltage imaging	9
2.3 Light patterning.	9
2.3.1 Light modulation	9
2.3.2 Microscope configuration	10
2.4 Image processing	11
2.4.1 Most common image analysis algorithms	11
2.4.2 Fluorescent label-free images	11
2.4.3 Brightfield and phase-contrast microscopy	11
2.5 Artificial intelligence	14
2.5.1 Motivation to use machine learning	14
2.5.2 General concept of neural networks	14
3 Methods	15
3.1 Programming language and choice of software	15
3.1.1 Programming language	15
3.1.2 Manual cell segmentation	16
3.1.3 Cell segmentation using conventional methods	17
3.1.4 Selecting an AI-based open software.	17
3.1.5 Cell segmentation using Cellpose and CellProfiler	18
3.1.6 Training a Cellpose model	18
3.1.7 Estimating segmentation accuracy.	19
3.2 Hardware synchronization	22
3.2.1 Technical specifications	23
3.2.2 Assessing recording quality	23
3.2.3 Measuring SNR	23

4	Results and Discussion	25
4.1	Algorithm accuracy	25
4.1.1	IoU and F-score	25
4.1.2	Dependence of segmentation accuracy on the number and size of ROIs	26
4.1.3	Potential improvements	27
4.2	Protocols for fast laser switching experiments.	27
4.3	SNR measurements in recordings	27
5	Conclusion	29
5.1	Proposed applications	29
5.2	Next steps	30
	Acknowledgements	31
	Bibliography	32
	Appendix 1. IoU and F-score Measurements	37
	Appendix 2. Microscope Setup Manual	38
	Appendix 3. DMD Projection Manual	39
	Appendix 4. Fast Switching Recording Manual	40

ABSTRACT

The study of the electrophysiological properties of neurons has reached a new level thanks to recent techniques that combine knowledge from different fields of science. For a method such as all-optical electrophysiology, the quality of cell segmentation in the image has one of the critical roles since the accuracy of illumination and perturbation of cells depends on it. The task is challenging because neurons have a complex morphology, and therefore traditional image analysis methods cannot perform accurate segmentation. This project focuses on building two AI-based models for neuron soma detection and mask prediction. Also, the project considers such an essential aspect of the experiment as the quality of the image recordings.

To implement the task, an open-source software Cellpose was chosen. Two algorithms for images acquired using fluorescence and phase-contrast microscopy were trained, and their efficiency was characterized by the Intersection over Union and F-score metrics. The resulting models demonstrated high performance. In addition, the signal-to-noise ratio was measured for recordings with different parameters such as camera read-out speed, illumination intensity, and frequency of laser switching.

Developed models are ready to be applied to the images of cells with or without fluorescent labels, although expanding the training dataset is recommended for improving segmentation accuracy. The project can be extended to detect and segment dendritic trees and spines to gain new insights into the subtle process of intercellular communication.

1

INTRODUCTION

Recent advances in protein engineering, photonics, and artificial intelligence provide a wide range of tools for state-of-the-art neuroscience research. The multidisciplinary approach currently facilitates *in vivo* and *in vitro* electrophysiology experiments, realistic disease modeling, and exploration of neural connectivity.

All-optical electrophysiology is one of the sophisticated methods to study neural circuit dynamics: it allows changing cell membrane voltage by light stimulation. The main principle behind this technique is to perturb a cell that expresses light-sensitive proteins by laser illumination of one wavelength and then record changes in transmembrane voltage, as the reporter protein will change the fluorescence intensity level upon laser illumination of another wavelength. It is also possible to stimulate one cell and record others - spatial resolution is achieved via projecting desired patterns via digital micromirror device (DMD). All-optical electrophysiology has an advantage over invasive methods such as patch-clamp, when the membrane needs to be disturbed to inject current into a cell. Complex methods face complex challenges, and all-optical electrophysiology is not an exemption. Recordings at high frame rates come with the price of reduced field of view and increased noise on the images; sample illumination with a laser of high intensity induces photodamage. These difficulties are tackled effectively by introducing modern electronics and bringing modifications to the structure of actuator and sensor proteins, which have been derived from light-sensitive bacterial rhodopsins.

An additional point of improvement is finding a way to produce an accurate illumination pattern - this is the main objective of this project. To create a projection, cell masks are manually drawn based on a widefield image, and then these masks are transformed into the DMD coordinates. Clearly, manual cell segmentation is imprecise and cumbersome, especially while working with complex-shaped cells like neurons. For the same reason, traditional image analysis methods fail as well, so it has been decided to use machine learning to perform this task.

This report is separated into chapters. The Theory chapter provides all information necessary for understanding the purpose and results of this project, including biological, physical, and computational perspectives. This part explains the cell model, principles

behind the action potential, and differences between actuator and sensor proteins, then delve into the concept of spatiotemporal patterning, finishing with image analysis algorithms along with relevant background on artificial intelligence.

In Methods, different cell segmentation algorithms are presented, explaining the choice of the particular software, and metrics for evaluating the model performance are given. Also, the concept of fast laser switching is elaborated, and signal-to-noise ratio measurements are explained.

The Results and Discussion chapter reports findings within this project and describes achieved accuracy in cell segmentation by the machine learning algorithm, suggesting potential improvements.

Finally, an overview is given in the Conclusion, followed by recommendations and suggestions for a possible project extension.

2

THEORY

All-optical electrophysiology is a complex topic that combines knowledge from multiple scientific domains - molecular and cell biology, physics and optics in particular, and computer science. Such multidisciplinary research requires relevant expertise and broad background. Therefore, the Theory chapter is intended to familiarize the reader with each part of the project to ensure that every aspect is evident and contributes to understanding this thesis's ultimate goal.

First, the biological part, the tissue model, presents the types of cells that can be used within this project. The next part introduces the concepts of optogenetics and voltage imaging, followed by the part describing the hardware for light patterning and cell recording. Subsequently, classical image analysis methods and the reasons for fluorescent label-free imaging are introduced. Finally, a concise description will introduce critical terms related to machine learning.

2.1. CELL MODEL

Cell cultures mimic plausible cell-to-cell interactions to facilitate *in vitro* experiments. Typically, cell culture is a process by which single cells are grown under controlled conditions (such as medium, temperature, gas concentration, pH) by the influence of specifically selected growth factors. In practice, the term "cell culture" refers mainly to the cultivation of single-tissue cells derived from multicellular eukaryotes, most commonly animals. For the disease modeling, cell cultures can be derived directly from the patients.

The primary cell cultures of this project are NPC-derived neurons and spiking HEK cells; the following section discusses the properties that made these cells suitable for all-optical electrophysiological experiments.

2.1.1. NEURONS

Nervous system contains two major types of cells - neurons and glial cells. Neurons can respond to various physical and chemical stimuli, as well as transmit nerve impulses,

while diverse types of glial cells are responsible for supporting neuronal functioning by providing nutrients, support, and protection from pathogens.

This Bachelor End Project focuses on imaging cells for all-optical electrophysiology; thus, the anatomy and basic properties of nerve cells will be discussed in this section. Most information contained in this subchapter is retrieved from Bear et al., 2015 and Purves et al., 2019 unless another source is stated.

2

Neuron anatomy

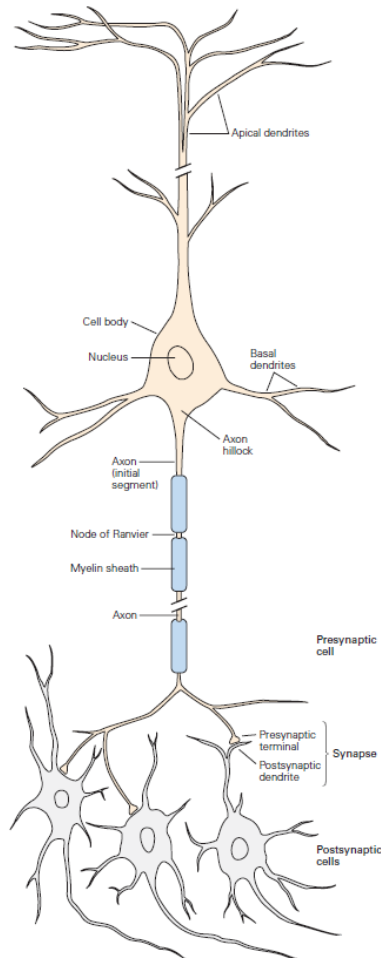


Figure 2.1: A simple representation of the neuron's principal structures. Image source: Kandel et al., 2021.

The simple model of a neuron is presented in Figure 2.1; there are three principal components: the cell body, also known as soma, and neurites - axon and dendrites - small tube-like structures radiating from the cell body. Soma contains the nucleus and

other organelles; this part is mainly responsible for protein synthesis in the cell. A particular structure called axon hillock gives rise to a single axon. Axon is a structure that conducts signals from soma to the next neuron via axon termini. The length of an axon might vary significantly, starting with hundreds of micrometers and up to about one meter. Often, axons are surrounded by a myelin sheath, which is formed by glial cells and increases the speed of impulse propagation.

Another type of neurites is dendrites, which also originate from the soma. Dendrites are receivers of impulses from other neurons, and in more detail, from other neurons' axon termini. The point of contact between the axon of one neuron and the dendrite neuron is called synapse; its structure will be discussed in the following subsection.

Neurons can be classified based on the number of neurites, the shape of the dendritic tree, functions, and many other parameters.

Synapse

Communication between neurons is established via signals transmitted through synapse (Figure 2.2). The impulse passes from the axon terminal of the presynaptic neuron, causing propagation of action potential. There are two types of synapses - electrical and chemical, and often they coexist withing an organism.

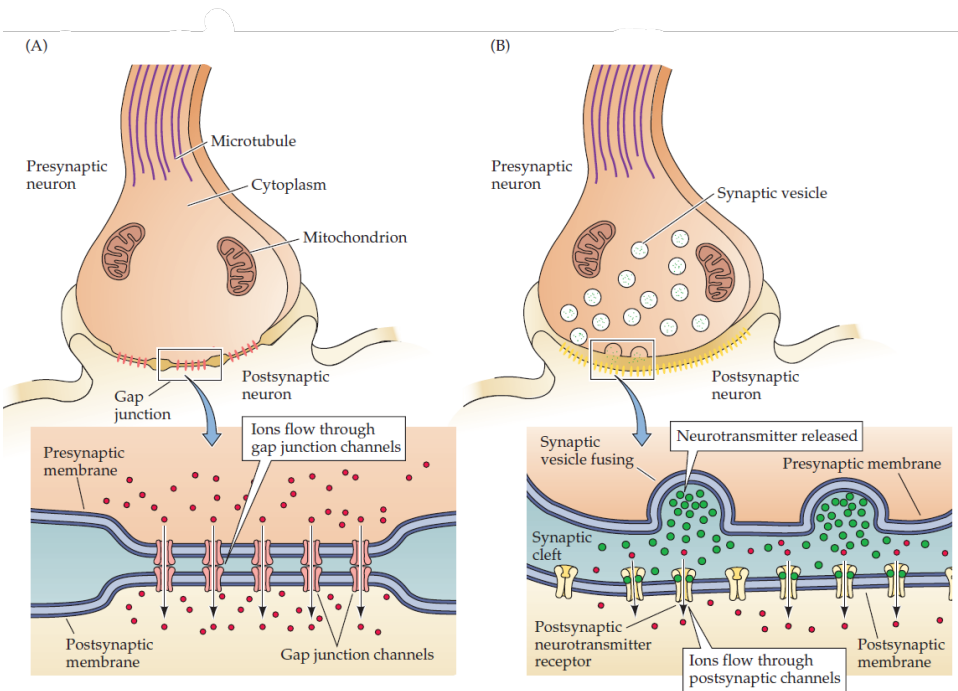


Figure 2.2: Synapse structure. a) Electrical synapse enables the ion flow via gap junctions - channels for physical cell connection; b) Chemical synapse establishes cell-to-cell communication via the neurotransmitter molecules. Image source: Purves et al., 2019.

Electrical synapse functions by passive ion flow through gap junction channels -

these synapses allow faster signal propagation and are considered less complex than chemical synapses. Signal propagation in a chemical synapse is realized through neurotransmitter release from the presynaptic membrane into the synaptic cleft. Consequently, these molecules bind to the specific receptors in the postsynaptic membrane, causing changes in the transmembrane voltage.

Action potential

One of the essential physiological properties of neurons is the ability to transmit electrical impulses, so-called action potentials; the scheme is shown in Figure 2.3. The mechanism behind action potential is based on changes in membrane potential due to the work of sodium-potassium pumps, potassium channels, and sodium channels. When the membrane is at rest with Na^+ and K^+ ions at equilibrium, the voltage across the membrane is approximately -70 mV. The cell membrane is selectively permeable, which means that passive channels allow an influx of sodium and outflux of potassium ions, which is compensated by the sodium-potassium pump.

Equilibrium is disturbed by binding neurotransmitter molecules to receptors on postsynaptic dendrite and Ca^{2+} influx during the nerve impulse propagation. This event opens voltage-gated sodium ion channels, and ions rush into the cell, causing rapid membrane depolarization. When the membrane potential reaches $+30$ mV - nearly the electrochemical equilibrium for sodium at the overshoot phase, Na^+ voltage-gated channels become inactive, while K^+ channels are activated, resulting in membrane repolarisation in the falling phase. After a short hyperpolarization phase, ion concentration returns to the initial state.

2.1.2. NEURON PROGENITOR CELLS

NPC-derived neurons is a convenient model that enables *in vitro* experiments with limited use of animal tissue, and disease modeling with the cells directly from patients. Understanding the nature of NPCs is necessary for grasping the idea and motivations behind this thesis. Thus, the following section briefly characterizes NPCs, their differentiation outcomes, research methods, and practical applications.

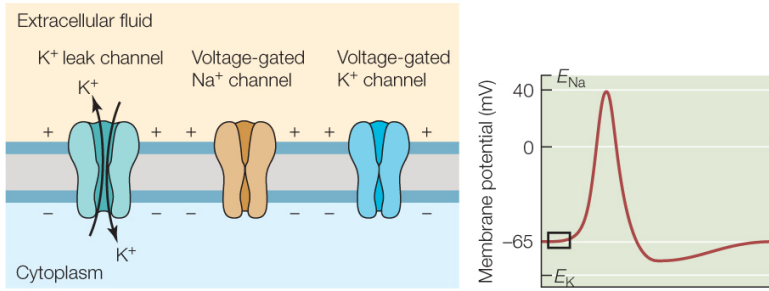
Overview

NPCs should be distinguished from stem cells based on their potency - the ability of the cell to differentiate into other cell types. Pluripotent stem cells can undergo an indefinite number of divisions and give rise to various cell types, while NPCs are multipotent cells with limited differentiation potential as they can divide only into glial and neuronal cells (Martínez-Cerdeño and Noctor, 2018).

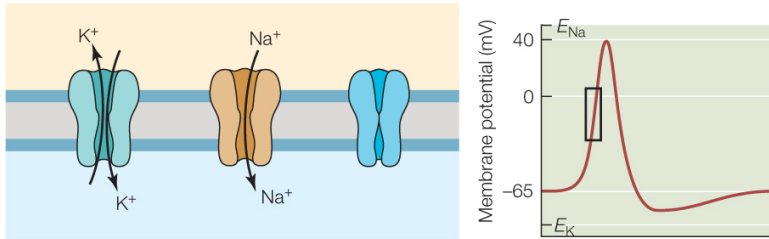
During the embryonic development in vertebrates, the proliferation of NPCs is mainly controlled by Sonic Hedgehog and Wnt/ β -catenin signaling pathways and Noggin protein (Tropepe et al., 2001), but numerous growth factors can influence cell fate depending on its spatial identity (Jessell, 2000; Farkas and Huttner, 2008).

For *in vitro* experiments, NPCs are derived from induced pluripotent stem cells (iPSCs). All the factors that might affect the cell fate determination are still unknown; existing neural induction protocols describe the expected ratio between neurons and glia using various reagents and procedures (Gunhanlar et al., 2017).

(A) Resting membrane potential



(B) Rising phase of action potential



(C) Falling phase of action potential

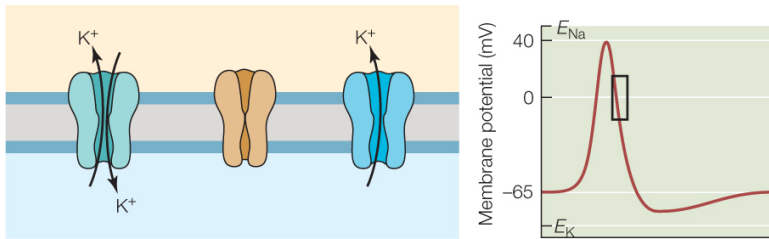


Figure 2.3: Action potential. a) Resting membrane - the transmembrane voltage between -65 mV and -70 mV is maintained by sodium-potassium pumps (active transport) and ion channels (passive transport); b) Rising phase is characterized by the rapid increase in the membrane potential upon cell stimulation; c) Falling phase is represented by the drop in transmembrane voltage due to the opening of voltage-dependent potassium channels. Image source: Hillis et al., 2013.

Practical application

NPCs-derived neurons and glia have multiple applications in different fields of study. Differentiation of neural progenitor cells upon various conditions allows gaining insights into healthy human brain development processes and modeling and studying diseases and conditions (Sidhaye and Knoblich, 2020; Das et al., 2020). Aside from understanding neural development, disease modeling is necessary for finding new drug treatment strategies (Porterfield and Porterfield, 2020).

Another promising area for NPCs application is stem cell therapy. For example, stroke, multiple sclerosis, and neurodegenerative diseases such as Alzheimer's disease and Parkin-

son's disease are associated with loss of neurons and glial cells, leading to disability. There is no efficient medicamental treatment for these conditions, and therefore transplantation of iPSCs and NPCs could alleviate the symptoms and improve patients' quality of life (Lindvall and Kokaia, 2006). Due to the relative novelty, ethical and legal complications related to this technology, large-scale clinical trials have not yet been launched, although the outcomes of early trials demonstrated positive results (Parmar et al., 2020; Curtis et al., 2018).

2.1.3. SPIKING HEK CELLS

HEK293T (Human Embryonic Kidney 293 - further referred to as HEK cells) cell culture is an immortalized lineage of cells that is convenient to maintain and transfect, therefore such tissue culture becomes a widely available instrument for multiple areas of research, including electrophysiological experiments. Modified HEK cells express potassium and sodium ion channels, which allows these cells to generate and propagate action potential. Necessary optogenetic components, namely actuator and sensor proteins (to be discussed in the next section), are also expressed.

2.2. ALL-OPTICAL ELECTROPHYSIOLOGY

All-optical electrophysiology combines the advantages of optogenetics and voltage imaging - two approaches for simultaneous optical excitation of the cell membrane and recording changes in membrane potential. Such a technique requires considerable effort, including careful selection of GEVIs to avoid cross-talk due to spectral overlap in actuators and reporters (Hochbaum et al., 2014), and development of a complex optical system for fast image acquisition with a maximal signal-to-noise ratio (SNR).

2.2.1. OPTOPATCH

Optopatch is a technique for perturbing cells using light stimulation via genetically encoded light-sensitive proteins. This method requires four principal components: cells with an optogenetic actuator and optogenetic sensor, along with pieces of hardware for spatial and temporal light patterning. The following subchapter and the Methods chapter will discuss each component in detail.

Actuators and sensors

Actuator proteins are able to activate or inhibit cell membrane potential in a non-invasive way. Light-sensitive ion channels in the membrane change their conformation in response to light stimulation, therefore controlling transmembrane voltage. Generally, actuators are represented by various types of genetically modified rhodopsins, for instance, channelrhodopsin-2 (ChR2), archaerhodopsin (Arch), or Channelrhodopsin from *Scherffelia dubia* (CheRiff) (Knöpfel, 2012).

Sensor proteins are needed for the detection of membrane potential. Voltage sensors such as Arch-derived mutated proteins QuasArs ('quality superior to Arch') alter their fluorescence intensity level depending on the transmembrane voltage and upon red light illumination. Co-expressed actuator and sensor protein pair - optopatch, Figure 2.4 - makes it possible to record of electrophysiological activity of the cell after its optoge-

netic stimulation (Hochbaum et al., 2014). To avoid confusion, it is important to state that in the context of this thesis terms “sensor”, “reporter” and “indicator” are used interchangeably, although there are subtle differences from the perspective of molecular engineering.

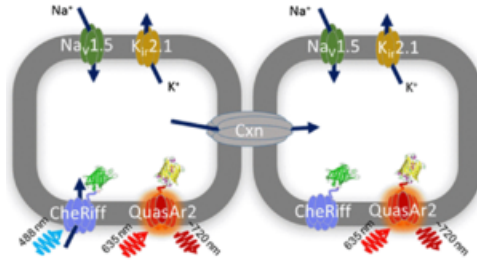


Figure 2.4: Schematic representation of a spiking HEK cell. Transgenic K⁺ and Na⁺ channels are responsible for the changes in transmembrane voltage. A cell can be perturbed by optical stimulation of CheRiff protein, and QuasAr protein reports changes in the voltage. Connexin (Cxn) connects cells, creating a gap junction. Image source: McNamara et al., 2016.

2.2.2. VOLTAGE IMAGING

Voltage imaging is another technique for recording the electrophysiological activity of a cell by visualizing changes in membrane voltage as changes in fluorescence intensity of specifically engineered proteins - genetically encoded voltage indicators (GEVIs).

Genetically Encoded Voltage Indicators

GEVIs create an opportunity for visualizing membrane action potentials upon stimulating selected cells. Thus they are suitable for studying interactions between cells on the neural circuit level. In most cases, the structure of voltage sensors is based on microbial opsins; different types of GEVIs vary in brightness, sensitivity, and response time (Knöpfel, 2012; Adam et al., 2019); hence appropriate proteins should be selected for particular experiments.

2.3. LIGHT PATTERNING

All-optical electrophysiology experiments demand accurate and fast illumination, which can be achieved by spatial and temporal light patterning realized by a sophisticated hardware setup.

2.3.1. LIGHT MODULATION

Precise illumination of targeted cells requires two types of light modulation: spatial and temporal. Spatial light modulator (SLM) directs light to the cells of interest for its stimulation. There are two types of SLMs - liquid crystal SLM (LC-SLM) and digital micromirror device (DMD). LC-SLMs are used for three-dimensional holographic photostimulation based on phase-shifted light (Anselmi et al., 2011), while DMD represents an array of mirrors, each mirror can change its position as “on” and “off” - this binary switch al-

lows to generate arbitrary light patterns faster than when using LC-SLM (Ronzitti et al., 2017; Packer et al., 2013). In this project, DMD will be used.

Spatial light modulation enables illumination and recording of the fluorescence intensity changes for specifically selected cells. To create a DMD projection, it is necessary to translate projecting area's corresponding camera coordinates to DMD coordinates. The process and importance of accurate cell segmentation and producing a mask are discussed in the following subchapter.

High temporal resolution can be achieved with an acousto-optical tunable filter (AOTF), which controls light wavelength and intensity via changing acoustic wave frequency (Murphy and Davidson, 2012).

2.3.2. MICROSCOPE CONFIGURATION

Custom-built microscopes for all-optical electrophysiology enable equipment adjustments based on the needs of a particular experiment, characteristics of a sample, and limitations in both hardware and samples, for instance, laser switching speed or GEVI sensitivity. This project uses wide-field illumination; the laser intensity can be regulated via an AOTF. DMD controls light patterning for illuminating selected parts of a sample, which is later recorded on a CMOS camera or photomultiplier tube (PMT). Figure 2.5 shows the main parts of a microscope setup (Meng et al., 2022).

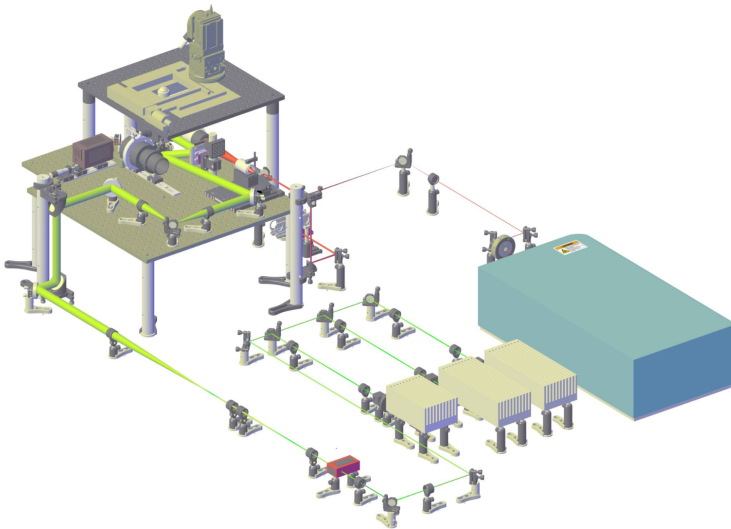


Figure 2.5: Microscope overview. AOTF-controlled laser beams of different wavelengths are combined and magnified by the system of lenses, then directed via DMD for sample illumination and detected by a CMOS camera. Graphics by Xin Meng.

All-optical electrophysiology demands significant effort - creating a tailored hardware setup and improving rhodopsins fluorescence intensity. Nonetheless, with recent

advances in optical and protein engineering, essential components can be adjusted for the needs of a particular experiment. It provides much freedom regarding various research that can be performed using this technique. For instance, one could shift their focus to large-scale recordings for investigating neural connectivity *in vitro* (Rickgauer et al., 2014), performing *in vivo* imaging (Packer et al., 2014), or studying rhodopsins on molecular level (Hochbaum et al., 2014).

Nevertheless, one more aspect remained unmentioned - software, which is a substantial part of the method as it controls DMD projections, AOTF and the camera. Further, the software is used for image pre- and postprocessing, particularly for creating masks that will be sent to DMDs and projected onto the cells for their photostimulation. The following subchapter discusses ways to obtain and analyze images, including traditional methods and machine learning.

2.4. IMAGE PROCESSING

This section describes methods for analysis of neuron, NPCs and HEK cells images. First, the most typical algorithms for the feature extraction will be discussed. Then, reasons for using unstained cells are given, followed by a comparison between brightfield and phase-contrast microscopy.

Choosing morphological features for image-based cell characterization might seem evident, but currently, visual parameters that allow accurate cell detection and segmentation remain unknown. Therefore, it is reasonable to track cells throughout their development to estimate cell motility and proliferation rate; also, considering a time dimension will provide additional information for more accurate analysis (Cohen et al., 2010). Hence, selecting criteria for cell quantification is a part of this project.

2.4.1. MOST COMMON IMAGE ANALYSIS ALGORITHMS

Cell state quantification requires multiple steps such as cell segmentation, image alignment for time-lapse frames, and further analysis. Compared to image analysis for most cell types, the task becomes more difficult due to the complex shape of neurons. Table 2.1 provides a summary of the most common methods used for analyzing neuron images (M. Winter et al., 2011; M. R. Winter et al., 2015; Al-Kofahi et al., 2006).

2.4.2. FLUORESCENT LABEL-FREE IMAGES

A small part of this project is dedicated to analyzing images obtained without fluorescent tags. Many modern techniques, including immunostaining or genome modifications for fluorescent protein expression, are widely used in scientific research. Confocal microscopy or multiphoton microscopy provide an opportunity to obtain high-resolution images. However, these methods have limitations because fluorescent labeling may require cell fixation, disturb the cellular environment, and induce photodamage.

2.4.3. BRIGHTFIELD AND PHASE-CONTRAST MICROSCOPY

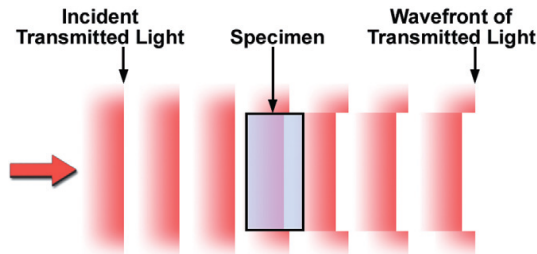
The choice to study unstained cells offers two available imaging options: brightfield microscopy and phase-contrast microscopy. Initially, brightfield microscopy was the preference for this project since it is a relatively simple method for cell imaging; however, it

Task	Method and description	Advantages	Disadvantages
Preprocessing	Gaussian blur: low-pass filter with Gaussian distribution attenuates high frequency signals.	The extent of image “smoothness” can be controlled by changing the standard deviation σ .	Attenuates both noise and signal and blurs cell structures.
	Morphological smoothing: opening operation followed by closing.	Removes dark and bright small artifacts from the image.	Can produce artifacts if noise is present at the cell edges.
Segmentation	Watershed transformation: selecting local intensity minima and expanding boundaries of an object.	Efficient for splitting touching cells and estimation the number of cells.	Requires a lot of preprocessing and often leads to oversegmentation.
	Otsu’s thresholding: minimizing intra-class variance using the intensity histogram.	High accuracy upon satisfying the conditions.	Works well only for a bimodal distribution of pixel intensities.
	k-means clustering: classifying pixels into k clusters based on intensity.	A relatively simple algorithm that is applicable to large sets of data.	Fails in case of complex cell morphology; automatic determination of k is problematic.
	Gaussian mixture model: a generalized k-means method that involves the variance of parameters.	More accurate segmentation due to assuming a non-circular cluster shape.	Requires multiple parameters, and needs to perform k-means as preprocessing.
Cell tracking	Nearest neighbor: assigning the same trajectory to objects based on their location on the previous frame.	A simple algorithm that allows measuring cell motility.	Fails with high cell density or noisy signal.

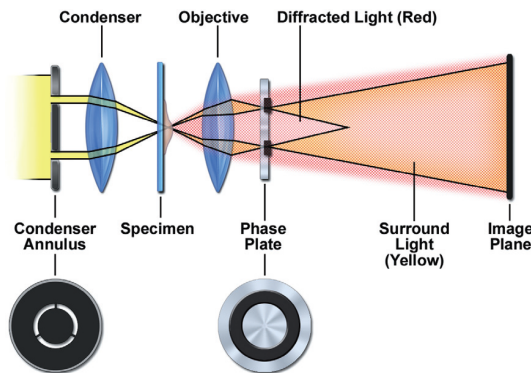
Table 2.1: Conventional image analysis methods applicable to cell images(Wu et al., 2008; Sonka et al., 1993).

produces low-contrast images that are difficult to process. Furthermore, only very few equivocal studies use brightfield microscopy for NPCs image analysis (Jiang, Wang, Gao, et al., 2016; Jiang, Wang, Luo, et al., 2016), concluding that more advanced techniques should be applied.

Phase-contrast microscopy allows imaging of even transparent specimens without fixation and staining. The technique is based on the phase shift when light rays pass through the sample. Waves that pass through the specimen but do not interact with it - undiffracted, or surrounding light, as well as diffracted waves, are both collected by the objective and undergo interference; therefore, the amplitude of the resulting wave changes, leading to the changes in light intensity and forming an image.



(a) Phase difference between diffracted light that passed through the specimen and undiffracted, surrounding light. As it can be seen, there is a phase delay of diffracted light.



(b) Main elements of phase-contrast microscope and light paths. Condenser annulus creates a hollow cone of light for sample illumination; phase plate advances the phase and reduces the amplitude of undiffracted light

Figure 2.6: Principles behind phase-contrast microscopy. Image source: Murphy and Davidson, 2012.

The difference between a brightfield and a phase-contrast microscope lies in two additional components of the latter: a condenser annulus and a phase plate. Condenser annulus is an annular diaphragm, and it is used to create oblique illumination of a sample. Undiffracted light forms a bright image of the condenser annulus in

the rear focal plane of the objective, the so-called diffraction plane. At the same time, diffracted rays pass the diffraction plane in multiple locations depending on the sample properties; the light path is depicted in Figure 2.6a.

The phase plate alternates phase and amplitude of undiffracted light. It is possible due to the construction of a phase plate: the dark ring on a phase plate (Figure 2.6b) represents the part with reduced thickness for surrounding light; thereby, the phase shift occurs. This dark ring is often coated with a metal film to reduce the amplitude of undiffracted light waves and achieve a high contrast image.

2.5. ARTIFICIAL INTELLIGENCE

Machine learning is used in this project as a tool for cell segmentation; this subchapter presents motivation to use it over traditional methods and a brief overview of an idea behind artificial neural networks.

2.5.1. MOTIVATION TO USE MACHINE LEARNING

As discussed previously, conventional methods for image analysis are imprecise and require close human supervision and active intervention. It makes the process of cell quantification very tedious, prone to errors, and thus unreliable, especially for a large amount of data and complex cell morphology. For this reason, machine learning is used more often in microscopy image analysis as a convenient tool for cell segmentation.

2.5.2. GENERAL CONCEPT OF NEURAL NETWORKS

An artificial neural network (NN) is represented by a set of artificial neurons, organized in layers and connected by so-called edges, each of which has its weight. Every neuron is a mathematical function that receives one or multiple inputs from the previous layer, like dendrites, and then produces a single output for the next layer, with an analogy to an axon of a biological neuron.

Initially, weights of edges are assigned randomly. During machine learning, or NN training, these weights are adjusted to minimize a loss function - the difference between produced and expected output. Transfer learning is a method to define the initial weights by an already trained NN for a similar type of task. For instance, a model trained to recognize bicycles can be used to initialize weights for a model for scooter detection. Such an approach accelerates the training process for a new model and reduces the data needed for training (Zhuang et al., 2019).

Another fundamental conception is supervised machine learning, which means that the algorithm maps input-output data based on manually labeled examples. This project uses supervised transfer learning to create cell masks for phase-contrast and fluorescence microscopy images.

3

METHODS

This chapter describes the process of selecting an appropriate way to reach the maximal accuracy in cell segmentation. Provided examples illustrate differences between image analysis tools, including manual segmentation via ImageJ, automatized Python code using classical methods, and machine learning-based open software. Then, the neural network training process is described. The last part of this chapter is dedicated to optimizing hardware and software to obtain high-quality images.

3.1. PROGRAMMING LANGUAGE AND CHOICE OF SOFTWARE

Cell segmentation is a specific task yet widely used in multiple domains. Therefore, there are numerous approaches to detecting and segmenting images depending on object characteristics such as type, density, morphology, etc. This subchapter provides reasons behind the choice of a particular programming language and software for creating accurate masks of neurons based on fluorescent and phase-contrast images.

3.1.1. PROGRAMMING LANGUAGE

Python is the programming language chosen for this project. This programming language is currently used in the lab; thus, other members can use the application, easily read and edit the code in the future.

Moreover, Python allows work with various packages - third-party software for specific purposes. In our case, working with machine learning and processing big datasets requires GPU-accelerated computations that involve the usage of a hybrid platform CUDA, supported through libraries such as CuPy and Numba.

The software evaluation is performed by segmenting cell somas on two sample images shown in Figure 3.1, representing typical data obtained during all-optical electrophysiology experiments.

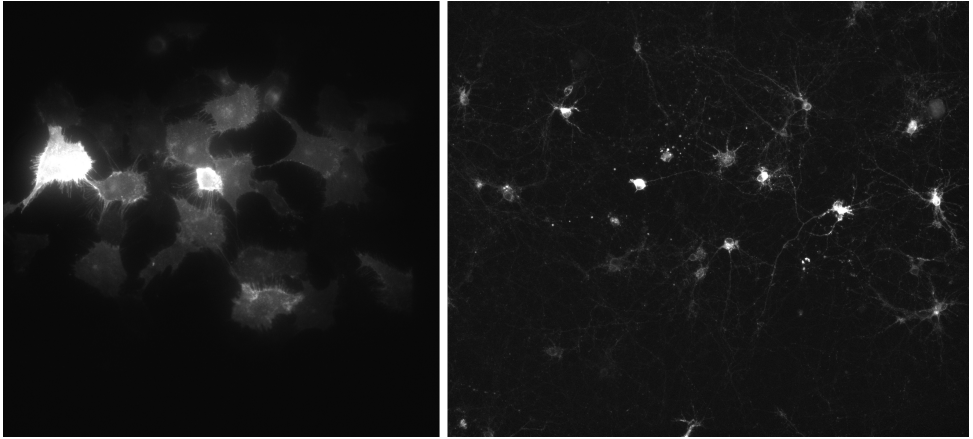


Figure 3.1: NPC-derived neurons expressing GFP, magnification 27.8 and 10.

3.1.2. MANUAL CELL SEGMENTATION

ImageJ (Schneider et al., 2012) is a convenient image analysis tool for life scientists - it includes many pre-installed plugins and allows one to create own macros using JavaScript. The programming language is one of the drawbacks, as it is incompatible with the software already used in the lab. Moreover, manual cell segmentation is subjective and inaccurate, and processing a large amount of data is tedious and time-consuming. Figure 3.2 confirms that images with manually selected parameters have numerous debris and are segmented inaccurately.

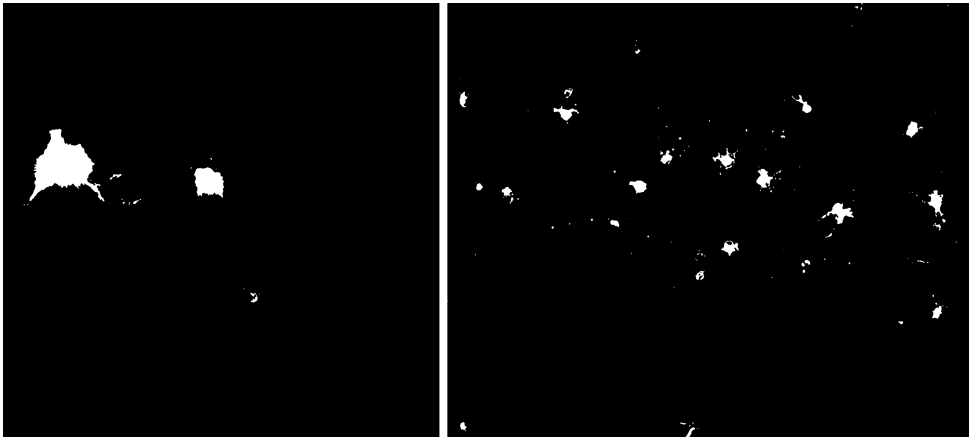


Figure 3.2: Test images after applying Gaussian blur, morphological smoothing, and Otsu's thresholding. Multiple somas were not detected, and segmentation artifacts were present.

3.1.3. CELL SEGMENTATION USING CONVENTIONAL METHODS

Automatic segmentation using classical methods in Python also demonstrates poor performance - Figure 3.3 shows that cells are either under-segmented or undetected. Detection algorithms are mostly based on mathematical morphology features; thus, this task remains a challenge due to the complex morphology and high cell density. Used code can be found on Brinks lab's GitHub: https://github.com/Brinkslab/Neuron_Image_Processing.

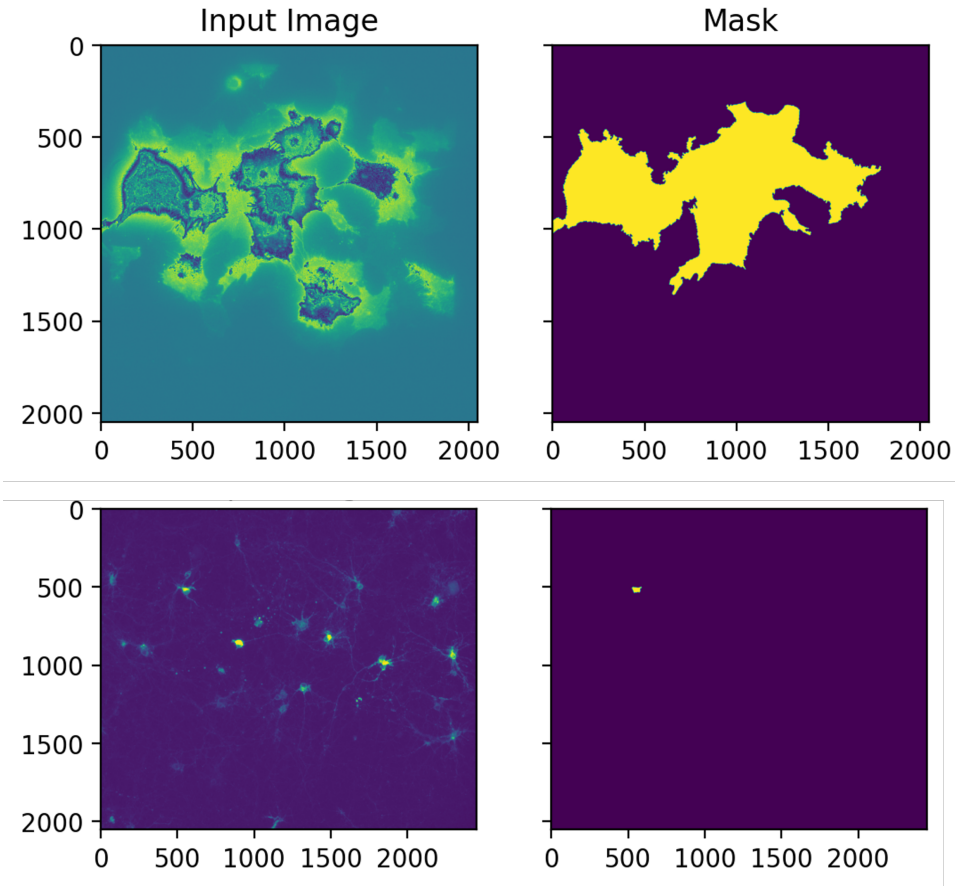


Figure 3.3: Neuron masks created using traditional image analysis methods in Python.

3.1.4. SELECTING AN AI-BASED OPEN SOFTWARE

There is much available software designed to segment cells, including neurons. These algorithms are developed using either artificial intelligence or various classical image analysis methods; performance and other characteristics may also vary.

To achieve tangible results, it has been decided to compare open software, as it might outperform and be more convenient than the algorithm currently used in this project. The following criteria were selected:

- Free and open-source software - in most cases, commercially available solutions are too costly. Moreover, it is not possible to modify or embed the code into existing software for all-optical electrophysiology experiments due to potential issues with licensing;
- Python as a programming language - chosen software must be compatible with software that is currently used to control the microscope; it will allow incorporating the algorithm into existing code;
- Accuracy - considering neurons' complex shape, cell segmentation accuracy is the main criterion. In the future, the project will be applied to the segmentation of not only neuron somas but also a dendritic tree, which requires a high-precision algorithm;
- Computational performance is a parameter that is commonly worth considering, but in this context, it is not crucial because the used GPU is powerful enough to perform segmentation tasks in a short time;
- It would be a significant advantage if the same program could be applied to images of label-free cells. However, this is purely optional due to considerable differences between fluorescence and phase-contrast images.

Most Python-based open software that would be suitable for processing images of cells with complex morphology, such as NeuroMorphoVis or Neuronize, is targeted at 3D images or skeletonized neurons. Therefore, it has been decided to focus on two generalists, deep learning-based algorithms: Cellpose 2.0 (Stringer and Pachitariu, 2022) and CellProfiler 4 (Stirling et al., 2021).

3.1.5. CELL SEGMENTATION USING CELLPOSE AND CELLPROFILER

As discussed in the previous section, both Cellpose and CellProfiler fulfill the requirements listed above; both have pre-trained models and a possibility for the user to train custom models. Yet, the results of test image segmentation shown in Figures 3.4 and 3.5 suggest proceeding with Cellpose for two reasons - accuracy of object detection and amount of debris.

While object detection accuracy is an apparent criterion for creating a cell mask, the absence of debris is crucial for cell perturbation by optical stimulation because accidental DMD projection of debris might cause undesirable changes in cell transmembrane voltage.

3.1.6. TRAINING A CELLPOSE MODEL

One of the advantages of Cellpose is a convenient interface for customizing a model for cell segmentation based on a “human-in-the-loop” pipeline - direct interaction between a machine learning algorithm and a human by providing immediate feedback on the segmentation result (see Figure 3.6). The training procedure is the following: the first step is selecting a model that has been trained on a similar task. Cellpose suggests several models provided by Model Zoo (Ramesh and Chaudhari, 2021) - an open platform for deep learning researchers that allows access to a wide range of already trained models.

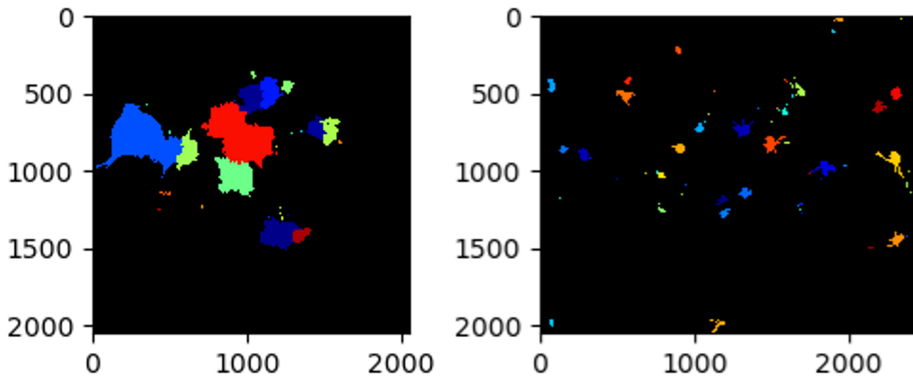


Figure 3.4: Neuron masks created using CellProfiler 4.

Next, the software requires loading one image from the dataset, applying the pre-trained algorithm to the image, and then manually correcting defined masks. This step repeats for every image in the training dataset. As mentioned before, such an approach requires less time, effort, and data than classical machine learning methods (Stringer and Pachitariu, 2022). Within this project, two models based on two microscopy methods were trained and evaluated.

Fluorescence microscopy images

The model for detection and segmentation of fluorescent cells has been trained on 50 images of neurons expressing GFP, obtained with the objective Olympus XLPLN25XWMP2, NA1.05, working distance 2.0mm, with a total magnification 27.8.

Phase-contrast microscopy images

As stated in the Theory chapter, phase-contrast is a preferred imaging technique for cells without fluorescent labels, compared to brightfield microscopy. Figure 3.7 shows that extracting information from brightfield images is highly problematic, if possible.

The model for phase-contrast images has been trained on 35 images, 30 of which were captured with the microscope MShot MF53-N, phase-contrast objective Plan20X/0.45NA, working distance 5.0mm. Another 5 images were retrieved from Christiansen et al., 2018 and acquired with Nikon S Plan Fluor 20X/0.6NA.

3.1.7. ESTIMATING SEGMENTATION ACCURACY

As with any method, cell segmentation performance can and should be quantified. There are many various metrics for this task; the majority of them are based on four main pixel classes, which are shown in Figure 3.8: true positives (TP), true negatives (TN), false positives (FP), and false negatives (FN).

Based on this classification, it is possible to find the Jaccard similarity coefficient (JCS), receiver operator characteristic curve, the Hausdorff index, the F-score, and others (Chen, 2021). In this project, the JSC, also known as the Jaccard index or intersection over union (IoU), is used to measure the overlap between the ground truth object T and

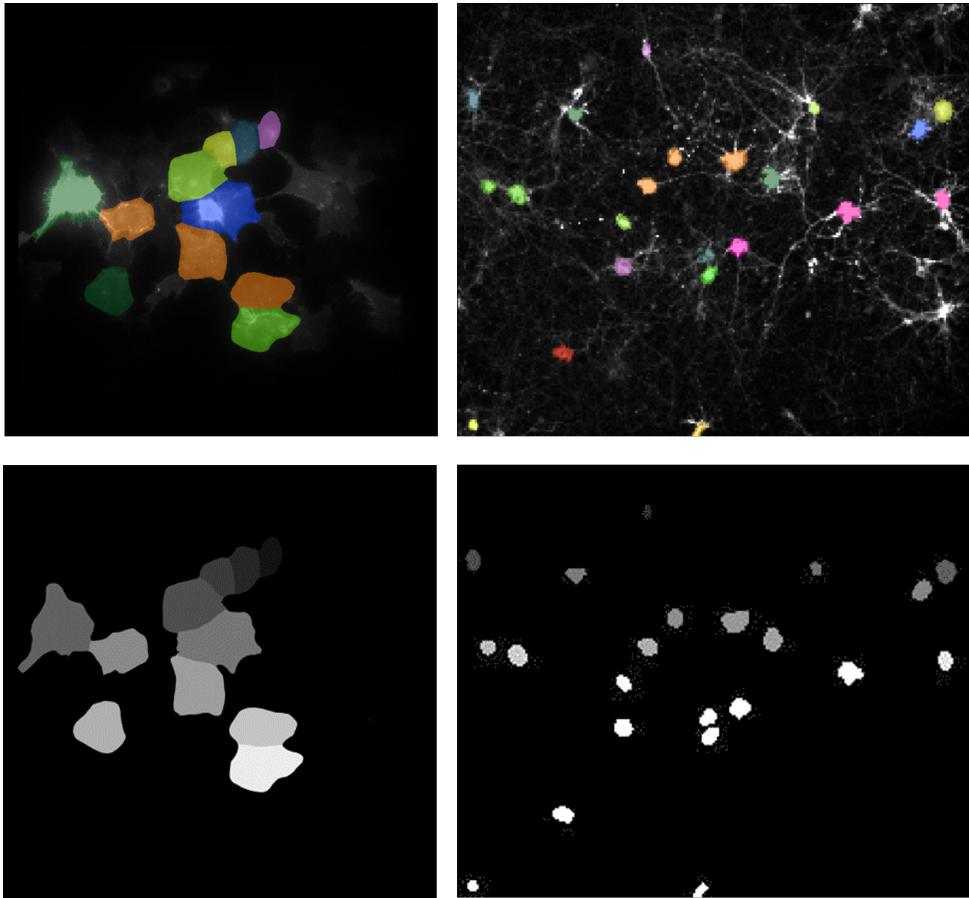


Figure 3.5: Neuron masks created using Cellpose 2.0. Top row: mask overlay, bottom row: resulting grey-scale masks.

segmented object S (Stringer et al., 2020). Object detection accuracy is estimated with F-score as a standard metric in computer vision. Both indicators can take a value from 0 to 1; higher numbers indicate more accurate segmentation.

Intersection over Union

Intersection over union is an average precision for estimating the match between segmented object and a ground truth: $AP = \frac{|TP|}{|TP|+|FP|+|FN|}$.

F-score

The F-score or F-measure, also known as the Dice similarity coefficient (DSC), is an accuracy measure based on precision and recall. Precision is a number that represents the fraction of true positive pixels in all positive pixels: $P = \frac{|TP|}{|TP|+|FP|}$, whilst recall is a fraction of true positive pixels in the true object: $R = \frac{|TP|}{|TP|+|FN|}$. In the literature, preci-

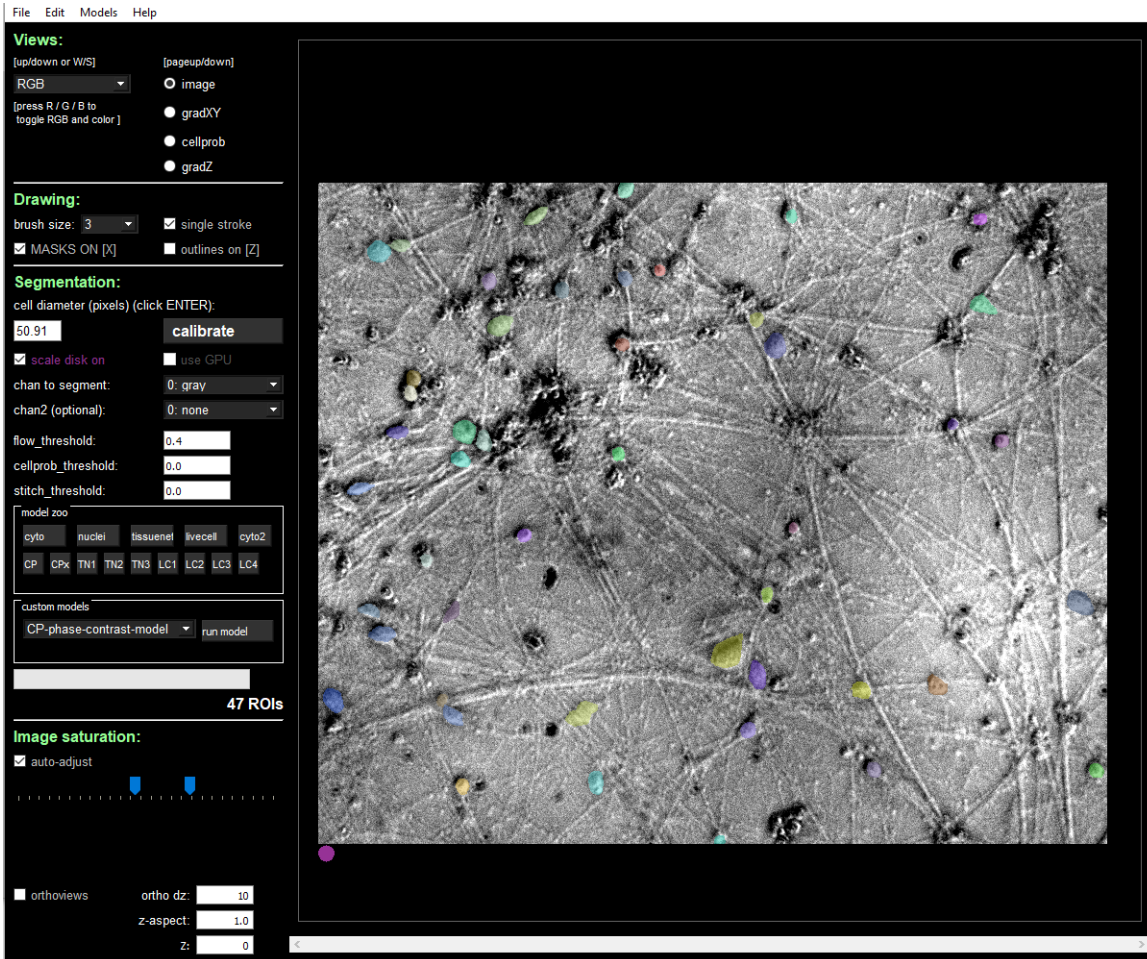


Figure 3.6: Cellpose GUI for cell segmentation and training an own model. The panel on the right allows selecting a channel for segmentation (RGB or greyscale); the drawing section defines parameters for manual cell segmentation, indicating cell diameter is needed for more precise automatic segmentation. Model Zoo suggests pre-trained models; otherwise, it is possible to load custom models; image saturation can be adjusted either manually or automatically; bottom parameters are defined for Z-stack analysis.

sion might be referred to as positive predictive value and recall as sensitivity. The F-score is the harmonic mean of the precision and recall $F = 2 \cdot \frac{P \cdot R}{P + R}$.

These metrics are helpful in model characterization and comparing it with other machine learning algorithms. It is essential to mention that ground truth masks were user-defined, meaning that the human factor can influence final numbers because objects are not defined with subpixel accuracy.

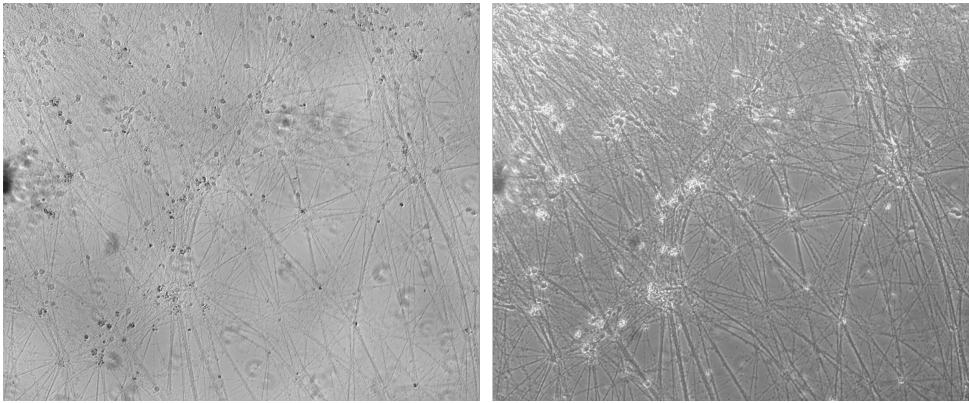


Figure 3.7: Comparison between images of NPCs obtained with brightfield (left) and phase-contrast (right) microscopes, magnification 10x.

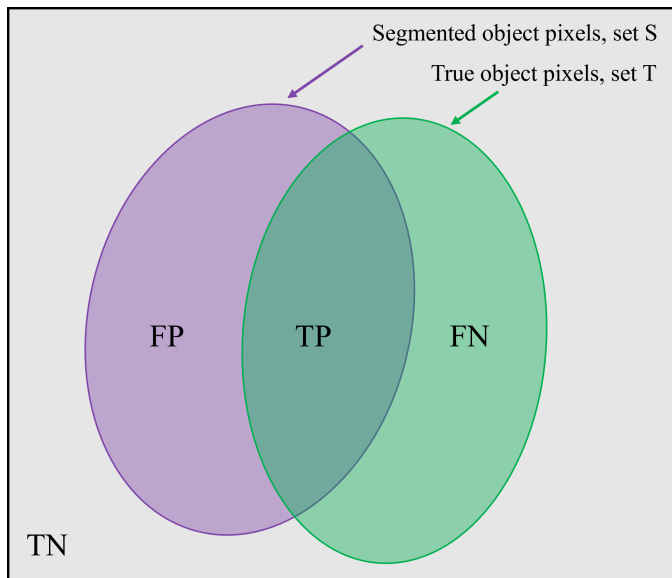


Figure 3.8: Representation of pixel classification. TP is a class of pixels correctly segmented as an object, TN - pixels correctly segmented background, FP - pixels incorrectly segmented as an object, FN - pixels incorrectly segmented as background.

3.2. HARDWARE SYNCHRONIZATION

There are multiple pieces of hardware to manage during cell recording: camera, lasers of different wavelengths, AOTF, and DMD. In order to synchronize these parts, waveforms are configured via specifically designed Python software to control temporal and spatial resolution. Figure 3.9 shows the general idea behind generating waveforms.

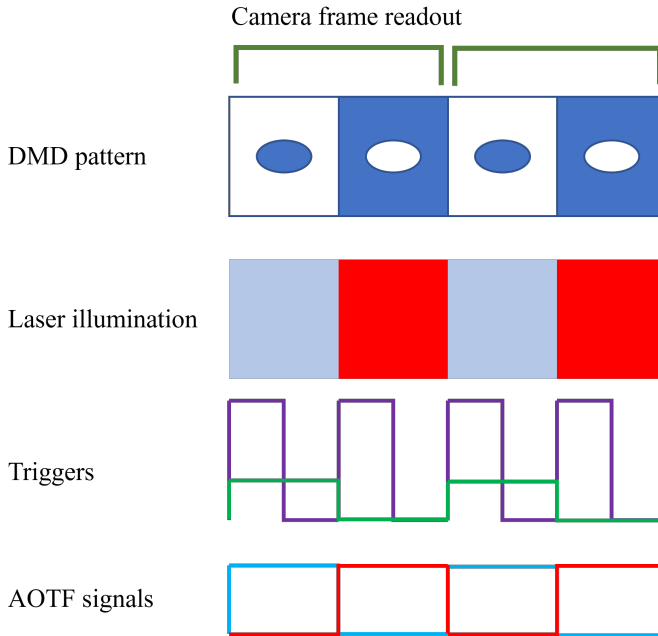


Figure 3.9: Wave configuration for all-optical electrophysiology recording. DMD switching is synchronized with laser illumination, which is, in turn, controlled by AOTF signals. It allows to perturb cell with the light of one wavelength and record another cell upon other wavelength illumination. The trigger represented as a purple line is a DMD switch trigger; the green line corresponds to the camera trigger - the camera is exposing in the reporter channel (Arch emission filter). Graphics by Xin Meng.

3.2.1. TECHNICAL SPECIFICATIONS

In this project, the following pieces of hardware were used: a sCMOS camera ORCA Flash4.0 V3, Hamamatsu; lasers MLL-FN-639, CNI and OBIS 488 LX, Coherent; AOTF nC-VI S, AA Optoelectronics; DMD Vialux V7001, Texas Instruments; input/output device USB-6363, National Instruments.

3.2.2. ASSESSING RECORDING QUALITY

Image quality is one of the crucial criteria for high-fidelity cell segmentation and quantification in general; therefore, recording parameters must be carefully selected in order to minimize noise. One of the experiments within this thesis's framework is dedicated to comparing two sets of parameters from the perspective of recording quality, which is characterized by the signal-to-noise ratio (SNR); these parameters can be found in Table 3.1 and Figure 3.10.

3.2.3. MEASURING SNR

Signal-to-noise ratio is a common metric to estimate image or video quality - it shows the ratio of a signal level to the background noise level: $SNR = \frac{\mu_{sig}}{\sigma_{sig}}$, Where μ is the average signal value, and σ is the standard deviation.

Set	Laser switching rate, Hz	640AO amplitude, V	Camera frame rate, fps	Duty cycle, %
Control	1000	5	2000	50
1	1000	5	1000	50
2	1000	2.5	500	100

Table 3.1: Settings for measurements 1 and 2. Doubled camera frame rate in the control recording is needed to confirm the fact of the laser switch - each frame captures the laser's "on" and "off" state, while it is impossible to see switching in the experimental recordings.

3

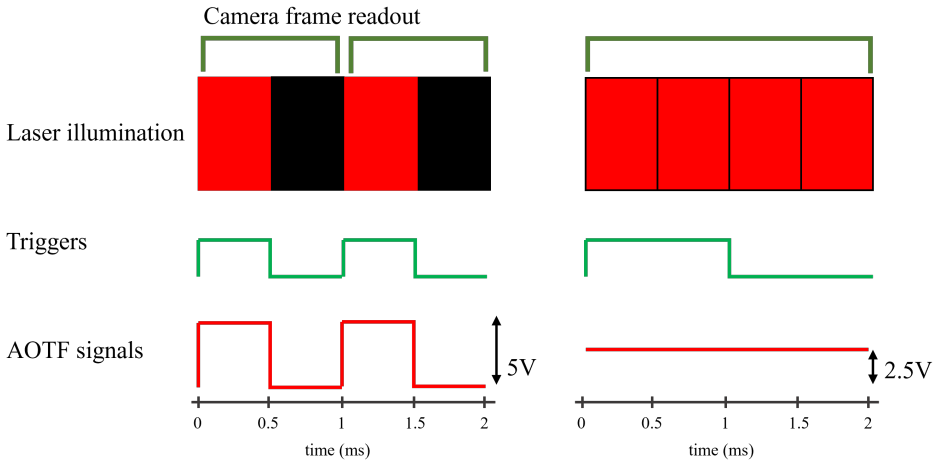


Figure 3.10: Wave configuration for set 1 (left) and 2 (right). The recording was made with full DMD projection and 640 nm laser as it is GEVI's emission wavelength.

Low-noise recordings have higher SNR, and noisy samples have low SNR, respectively. For measuring the SNR of an image, the following formula is used:

$$SNR = 10 \cdot \log_{10} \cdot \frac{\sum_0^{n_x-1} \sum_0^{n_y-1} [r(x, y)]^2}{\sum_0^{n_x-1} \sum_0^{n_y-1} [r(x, y) - t(x, y)]^2}$$

Where n_x and n_y are the image size in pixels, $r(x, y)$ are pixel values on a reference image, and $t(x, y)$ are pixel values of the test image. For the stack of images, SNR is measured individually for each frame. Typically, the SNR is measured in decibels (dB).

The SNR was measured using the ImageJ plugin developed by Sage and Unser, 2003.

4

RESULTS AND DISCUSSION

This chapter presents the results obtained within the project. First, the cell segmentation accuracy is evaluated based on metrics described in the Methods chapter. Additionally, the relation between a number of regions of interest (ROI), average cell size, and mask prediction accuracy are investigated. Then, fast switching recording protocols are presented, followed by the results of SNR measurements for two sets of parameters.

4.1. ALGORITHM ACCURACY

As the main result of this project, two AI-based algorithms were trained to detect and segment images of NPC-derived neurons captured with fluorescence and phase-contrast microscopes - the models are available on Brinks lab's GitHub: <https://github.com/Brinkslab>. The Fluorescence model is based on the pre-trained CP model available on Cellpose, the Phase-Contrast model has been trained with weights initiated by the LiveCell model (Edlund et al., 2021).

4.1.1. IOU AND F-SCORE

Tables 1 and 2 in the Appendix, and Figure 4.1 below present measurements for predicted masks and true (user-defined) masks for models trained on fluorescence and phase-contrast data. For each model, 10 additional images were segmented by the Cellpose algorithm, then by the user; the number of ROIs, mask areas in pixels, and the area of the mask overlap was calculated via ImageJ.

The average IoU values for the Fluorescence and Phase-Contrast models are 0.8345 (SD 0.0647) and 0.7757 (SD 0.0359) respectively; the F-scores are 0.9084 (SD 0.0386) and 0.8732 (SD 0.0227) with the same order.

Even though the Fluorescence model outperformed Phase-Contrast, both demonstrate reasonably good results. IoU less than 0.5 is considered poor image segmentation quality, values between 0.5 and 0.75 as good, and values above 0.75 as excellent. High F-score values also confirm that the cells are detected accurately (Chen, 2021).

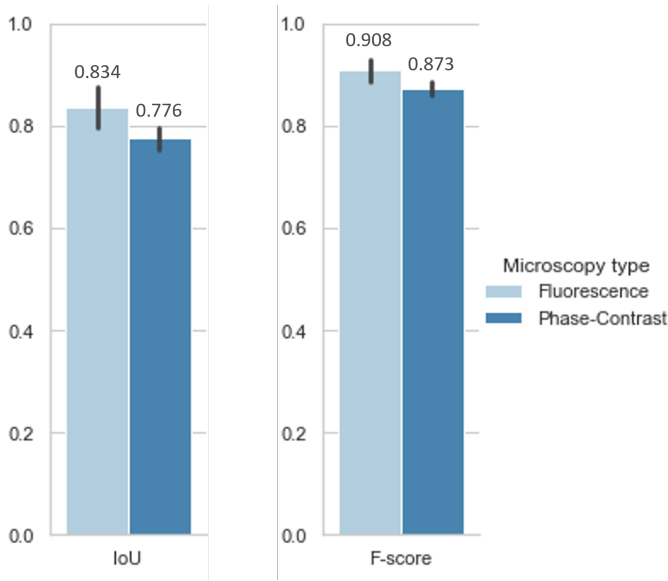


Figure 4.1: Comparison of cell mask prediction metrics for two models. Both IoU and F-score are higher for the algorithm trained on fluorescent image data, which means better performance in the cell segmentation task.

	Model			
	Fluorescence		Phase-Contrast	
	Number of ROIs	Avg ROI size	Number of ROIs	Avg ROI size
IoU	-0.59539	0.19467	0.04836	0.57483
F-score	-0.59096	0.19971	0.05569	0.57049

Table 4.1: Pearson correlation coefficients between IoU, F-scores, number, and an average size of ROIs for both models.

4.1.2. DEPENDENCE OF SEGMENTATION ACCURACY ON THE NUMBER AND SIZE OF ROIS

If there are more cells on the image and they are smaller, cell detection and segmentation tasks might become more difficult. Therefore, it has been decided to analyze whether there is a relation between mask prediction accuracy and ROI characteristics. Table 4.1 presents the Pearson correlation coefficient between various parameters.

The Pearson correlation is defined by the formula $\rho_{X,Y} = \frac{Cov(X,Y)}{\sigma_X\sigma_Y}$, with $Cov(X,Y)$ being the covariance between two datasets and the σ - standard deviation for each dataset. This coefficient measures the linear correlation between two datasets. It can take values between -1 and 1, where values below zero mean negative correlation, and above zero - positive; the larger the absolute value, the stronger the trend. However, one should remember that correlation does not always mean causation.

It is important to mention that data from both models differ - Tables 1 and 2 in the

Appendix show that training images for the Fluorescence model mostly had single large cells, and the Phase-Contrast model was trained on images with numerous small cells. There are two curious observations based on the table above. First, a fairly strong negative correlation is observed between the number of ROIs and segmentation accuracy for the Fluorescence model, e.g., the more cells there are on the image, the less accurate will be the task prediction. It can be explained by the difficulties in splitting touching cells and a strong halo effect inherent in images obtained using this type of microscopy.

The second observation is a relatively strong positive correlation between the average ROI size and accuracy metrics for the Phase-Contrast model and a weak positive correlation for the Fluorescence model, meaning that the segmentation task is performed more successfully for the cells of larger size. Limited image resolution might be a reason behind less precision in mask prediction for smaller objects.

While recognizing that the results are reasonable (Shen et al., 2018), there is not enough data to come to a firm conclusion. Testing set containing only 10 images per model might be sufficient to identify a general tendency, but not enough to define concrete numbers; therefore, expanding training and testing sets is recommended.

4.1.3. POTENTIAL IMPROVEMENTS

One of the advantages of Cellpose is the opportunity to continue custom model training at any moment in the future. More images with differing numbers, sizes, and densities of cells would improve segmentation quality. Yet, training on too much data should be avoided as this can lead to the model overfitting - an event when an algorithm erroneously treats background noise as data. Generally, overfitting occurs after processing hundreds of images, so it is not an issue within this project.

4.2. PROTOCOLS FOR FAST LASER SWITCHING EXPERIMENTS

All-optical electrophysiology experiments are often perplexing. One of the objectives of this project was to facilitate understanding and performing such experiments, including creating short manuals in an easy-to-follow manner. These protocols are intended to familiarize the user with the principle parts of hardware and guide them through setting up the experiment and configuring necessary parameters. The resulting protocols can be found in the Appendix.

4.3. SNR MEASUREMENTS IN RECORDINGS

Figure 4.2 presents the result of SNR measurements for two parameter sets from Table 3.1: 1000 fps camera frame rate with switching laser and 500 fps camera frame rate with constant red light illumination; each value is the average of the measurements over 500 frames.

The average SNR for set 1 is 23.887 dB (SD 0.0274), and for set 2 - 21.212 dB (SD 0.0309), both values are within an acceptable range for voltage imaging (Flytzanis et al., 2014).

In theory, the higher temporal resolution allows to distinguish sub-millisecond changes in the cell membrane voltage, but in practice, imaging rates higher than needed lead to

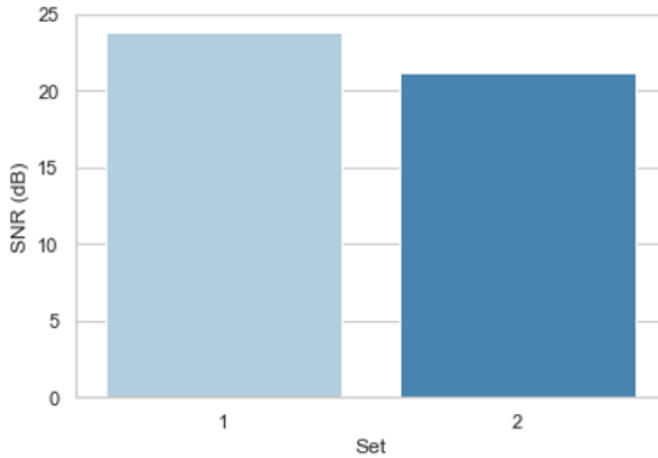


Figure 4.2: Results of SNR measurements. Set 1: 1000 Hz red laser switching with voltage 5V, duty cycle 50%, and camera frame rate 1000 fps; set 2: 1000 Hz red laser switching with voltage 2.5V, duty cycle 100% (constant illumination), and camera frame rate 500 fps.

the decrease of SNR, because it increases the readout noise (Quicke et al., 2019). Also, increasing the frame rate is coupled with the necessity to use higher laser intensity, which leads to sample photodamage.

Additionally, there is a trade-off between high frame rate and field of view, because a sCMOS camera readout starts from the center of the sensor and goes to the upper and lower halves simultaneously, so there must be enough time to scan all lines before the next trigger arrives. A higher frame rate means less time to scan all the rows, which, in turn, demands reducing FOV to a few tens of pixels, thereby complicating cell observation.

In the context of a real experiment with recording cells expressing GEVIs, the SNR value is expected to be lower because of the background fluorescence, especially with high cell density. Besides, there is still no GEVI that is fast, bright, and sensitive enough at the same time, but GEVIs with slower kinetics can be detected in the lower camera frame rate recordings, which means that they can be used in experiments when other characteristics are more important (Knöpfel and Song, 2019).

Overall, selected sets of parameters did not demonstrate significant differences in SNR between the two models, thus there is no universal answer - the camera frame rate, laser intensity, and spatiotemporal patterns should be selected according to the needs of a particular experiment, GEVI characteristics, cell culture density and desired field of view.

5

CONCLUSION

This project aimed to find an approach for accurate cell mask prediction for the images of NPC-derived neurons, explicitly designed for the needs of all-optical electrophysiology experiments. Based on the open Python software Cellpose, two deep learning-based models were trained to detect and segment neurons for fluorescence and phase-contrast microscopy images. Both algorithms demonstrated high performance according to appropriate metrics for estimating such tasks. Furthermore, a positive correlation is found between the improvement in the quality of segmentation for less and larger ROIs per image; however, minding that more test samples are needed to confirm this interconnection firmly.

Developed protocols for creating DMD projections, waveform configuration, and laser switching recording will assist the lab members in related experiments.

In the second part of the project, the SNR values were measured to estimate the quality of recordings with different spatiotemporal resolutions. Results confirmed that optimal parameters for waveform configuration vary depending on particular GEVI, recording time, desired FOV, and cellular processes that need to be distinguished.

5.1. PROPOSED APPLICATIONS

The Fluorescent model is ready to be applied to generate patterns for DMD projection. Alternatively, mounting a phase-contrast objective in the microscope for voltage imaging is strongly recommended as it will help to avoid photobleaching upon creating a cell mask.

The Phase-Contrast model can be applied to the field that is not directly related to voltage imaging - cell culture monitoring. NPC culturing is a tedious process that takes several months. Image-based cell quantification algorithms might assist in estimating cell state, health, and tracking proliferation, especially when cells are not yet transfected and cannot be monitored with fluorescence microscopy.

5.2. NEXT STEPS

SNR measurements as an approach to assessing recording quality can be utilized in future parameter optimization. Moreover, image SNR is expected to increase with the advancements in the Brinks lab's Protein Evolution Project - research for optimizing GEVI through directed evolution. As sample protein characteristics vary, one could consider exploring different spatiotemporal resolution parameters. Moreover, improving reporter protein sensitivity and brightness might be a starting point for lowering the intensity of red laser illumination, preventing cell photodamage.

Dendritic trees and spines segmentation is also relevant for voltage imaging (Popovic et al., 2015; Antic et al., 2016). These complex cellular structures participate in action potential propagation, and the ability to selectively perturb dendrites and spines will open a window of opportunity for more advanced neural connection mapping. The materials and results of this thesis can serve as a starting point for a new ambitious project in all-optical electrophysiology.

ACKNOWLEDGEMENTS

I would like to express my gratitude to my supervisor Daan Brinks and his lab for giving me the opportunity to do my thesis here, guiding me through the project, and giving me the freedom to explore my own ideas. Thank you for showing me that science is not only about knowing complex theories but mostly about being able to creatively apply them in practice.

Also, I want to thank Elizabeth Carroll for being a second examiner for my Bachelor End Project and assessing my work.

I am profoundly grateful to Xin Meng for the technical guidance, theoretical support, feedback and valuable advice, and to Qiangrui Dong for helping with cells. I appreciate Journal club discussions and coffee corner chats; thanks to the members of both Brinks and Carroll labs, especially to the inhabitants of the students' room, for creating a comfortable working environment.

Special thanks to my fellow nano Mai Phuong Nguyen Ngoc for thoughtful proofreading of my work and making valuable comments.

And, of course, I want to thank my family and friends for tremendous moral support, for being with me through all ups and downs - for making this project possible.

BIBLIOGRAPHY

- Adam, Y., Kim, J. J., Lou, S., Zhao, Y., Xie, M. E., Brinks, D., Wu, H., Mostajo-Radji, M. A., Kheifets, S., Parot, V., Chettih, S., Williams, K. J., Gmeiner, B., Farhi, S. L., Madisen, L., Buchanan, E. K., Kinsella, I., Zhou, D., Paninski, L., ... Cohen, A. E. (2019). Voltage imaging and optogenetics reveal behaviour-dependent changes in hippocampal dynamics. *Nature* 2019 569:7756, 569(7756), 413–417. <https://doi.org/10.1038/s41586-019-1166-7>
- Al-Kofahi, O., Radke, R. J., Goderie, S. K., Shen, Q., Temple, S., & Roysam, B. (2006). Automated Cell Lineage Construction: A Rapid Method to Analyze Clonal Development Established with Murine Neural Progenitor Cells. *https://doi.org/10.4161/cc.5.3.2426*, 5(3), 327–335. <https://doi.org/10.4161/CC.5.3.2426>
- Anselmi, F., Ventalon, C., Bèguea, A., Ogdenb, D., & Emiliani, V. (2011). Three-dimensional imaging and photostimulation by remote-focusing and holographic light patterning. *Proceedings of the National Academy of Sciences of the United States of America*, 108(49), 19504–19509. <https://doi.org/10.1073/PNAS.1109111108/>
- Antic, S. D., Empson, R. M., & Knöpfel, T. (2016). Voltage imaging to understand connections and functions of neuronal circuits. *Journal of Neurophysiology*, 116(1), 135–152. <https://doi.org/10.1152/JN.00226.2016/>
- Bear, M. F., Connors, B. W., & Paradiso, M. (2015). *Neuroscience : Exploring the Brain*. Jones & Bartlett Learning.
- Chen, M. (Ed.). (2021). *Computer Vision for Microscopy Image Analysis*. Elsevier. <https://doi.org/10.1016/C2017-0-01771-8>
- Christiansen, E. M., Yang, S. J., Ando, D. M., Javaherian, A., Skibinski, G., Lipnick, S., Mount, E., O'Neil, A., Shah, K., Lee, A. K., Goyal, P., Fedus, W., Poplin, R., Esteva, A., Berndl, M., Rubin, L. L., Nelson, P., & Finkbeiner, S. (2018). In Silico Labeling: Predicting Fluorescent Labels in Unlabeled Images. *Cell*, 173(3), 792–803. <https://doi.org/10.1016/J.CELL.2018.03.040>
- Cohen, A. R., Gomes, F. L., Roysam, B., & Cayouette, M. (2010). Computational prediction of neural progenitor cell fates. *Nature Methods* 2010 7:3, 7(3), 213–218. <https://doi.org/10.1038/nmeth.1424>
- Curtis, E., Martin, J. R., Gabel, B., Sidhu, N., Rzesiewicz, T. K., Mandeville, R., Van Gorp, S., Leerink, M., Tadokoro, T., Marsala, S., Jamieson, C., Marsala, M., & Ciacci, J. D. (2018). A First-in-Human, Phase I Study of Neural Stem Cell Transplantation for Chronic Spinal Cord Injury. *Cell Stem Cell*, 22(6), 941–950. <https://doi.org/10.1016/J.STEM.2018.05.014>
- Das, D., Feuer, K., Wahbeh, M., & Avramopoulos, D. (2020). Modeling Psychiatric Disorder Biology with Stem Cells. *Current Psychiatry Reports*, 22(5), 1–23. <https://doi.org/10.1007/s11920-020-01148-1>
- Edlund, C., Jackson, T. R., Khalid, N., Bevan, N., Dale, T., Dengel, A., Ahmed, S., Trygg, J., & Sjögren, R. (2021). LIVECell—A large-scale dataset for label-free live cell

- segmentation. *Nature Methods* 2021 18:9, 18(9), 1038–1045. <https://doi.org/10.1038/s41592-021-01249-6>
- Farkas, L. M., & Huttner, W. B. (2008). The cell biology of neural stem and progenitor cells and its significance for their proliferation versus differentiation during mammalian brain development. *Current Opinion in Cell Biology*, 20(6), 707–715. <https://doi.org/10.1016/J.CEB.2008.09.008>
- Flytzanis, N. C., Bedbrook, C. N., Chiu, H., Engqvist, M. K., Xiao, C., Chan, K. Y., Sternberg, P. W., Arnold, F. H., & Gradinaru, V. (2014). Archaelhodopsin variants with enhanced voltage-sensitive fluorescence in mammalian and *Caenorhabditis elegans* neurons. *Nature Communications* 2014 5:1, 5(1), 1–9. <https://doi.org/10.1038/ncomms5894>
- Gunhanlar, N., Shpak, G., van der Kroeg, M., Gouty-Colomer, L. A., Munshi, S. T., Lendemeijer, B., Ghazvini, M., Dupont, C., Hoogendijk, W. J., Gribnau, J., de Vrij, F. M., & Kushner, S. A. (2017). A simplified protocol for differentiation of electrophysiologically mature neuronal networks from human induced pluripotent stem cells. *Molecular Psychiatry* 2018 23:5, 23(5), 1336–1344. <https://doi.org/10.1038/mp.2017.56>
- Hillis, D. M., Sadava, D. E., Hill, R. W., & Price, M. V. (2013). *Principles of Life* (W. H. Freeman, Ed.). Macmillan Learning.
- Hochbaum, D. R., Zhao, Y., Farhi, S. L., Klapoetke, N., Werley, C. A., Kapoor, V., Zou, P., Kralj, J. M., MacLaurin, D., Smedemark-Margulies, N., Saulnier, J. L., Boulting, G. L., Straub, C., Cho, Y. K., Melkonian, M., Wong, G. K. S., Harrison, D. J., Murthy, V. N., Sabatini, B. L., ... Cohen, A. E. (2014). All-optical electrophysiology in mammalian neurons using engineered microbial rhodopsins. *Nature Methods* 2014 11:8, 11(8), 825–833. <https://doi.org/10.1038/nmeth.3000>
- Jessell, T. M. (2000). Neuronal specification in the spinal cord: inductive signals and transcriptional codes. *Nature Reviews Genetics* 2000 1:1, 1(1), 20–29. <https://doi.org/10.1038/35049541>
- Jiang, B., Wang, X., Gao, Q., Lin, Z., Zhang, R., & Zhang, X. (2016). Application of support vector machine to recognize trans-differentiated neural progenitor cells for bright-field microscopy. *Proceedings - 5th International Conference on Instrumentation and Measurement, Computer, Communication, and Control, IMCCC 2015*, 215–219. <https://doi.org/10.1109/IMCCC.2015.52>
- Jiang, B., Wang, X., Luo, J., Zhang, X., Xiong, Y., & Pang, H. (2016). Convolutional neural networks in automatic recognition of trans-differentiated neural progenitor cells under bright-field microscopy. *Proceedings - 5th International Conference on Instrumentation and Measurement, Computer, Communication, and Control, IMCCC 2015*, 122–126. <https://doi.org/10.1109/IMCCC.2015.33>
- Kandel, E. R., Koester, J., Mack, S., & Siegelbaum, S. (2021). *Principles of Neural Science* (Sixth edit). McGraw-Hill.
- Knöpfel, T. (2012). Genetically encoded optical indicators for the analysis of neuronal circuits. *Nature Reviews Neuroscience* 2012 13:10, 13(10), 687–700. <https://doi.org/10.1038/nrn3293>

- Knöpfel, T., & Song, C. (2019). Optical voltage imaging in neurons: moving from technology development to practical tool. *Nature Reviews Neuroscience* 2019 20:12, 20(12), 719–727. <https://doi.org/10.1038/s41583-019-0231-4>
- Lindvall, O., & Kokaia, Z. (2006). Stem cells for the treatment of neurological disorders. *Nature* 2006 441:7097, 441(7097), 1094–1096. <https://doi.org/10.1038/nature04960>
- Martínez-Cerdeño, V., & Noctor, S. C. (2018). Neural progenitor cell terminology. *Frontiers in Neuroanatomy*, 12, 104. <https://doi.org/10.3389/fnana.2018.00104>
- McNamara, H. M., Zhang, H., Werley, C. A., & Cohen, A. E. (2016). Optically controlled oscillators in an engineered bioelectric tissue. *Physical Review X*, 6(3), 031001. <https://doi.org/10.1103/PHYSREVX.6.031001>
- Meng, X., Huisman, L., Huijben, T., Szabo, G., Tol, R. v., Heer, I. d., Ganapathy, S., & Brinks, D. (2022). A compact microscope for voltage imaging. *Journal of Optics*, 24(5), 054004. <https://doi.org/10.1088/2040-8986/AC5DD5>
- Murphy, D. B., & Davidson, M. W. (2012). *Fundamentals of Light Microscopy and Electronic Imaging: Second Edition*. John Wiley; Sons. <https://doi.org/10.1002/9781118382905>
- Packer, A. M., Roska, B., & Häusser, M. (2013). Targeting neurons and photons for optogenetics. *Nature Neuroscience* 2013 16:7, 16(7), 805–815. <https://doi.org/10.1038/nn.3427>
- Packer, A. M., Russell, L. E., Dalgleish, H. W., & Häusser, M. (2014). Simultaneous all-optical manipulation and recording of neural circuit activity with cellular resolution in vivo. *Nature Methods* 2014 12:2, 12(2), 140–146. <https://doi.org/10.1038/nmeth.3217>
- Parmar, M., Grealish, S., & Henchcliffe, C. (2020). The future of stem cell therapies for Parkinson disease. *Nature Reviews Neuroscience* 2020 21:2, 21(2), 103–115. <https://doi.org/10.1038/s41583-019-0257-7>
- Popovic, M. A., Carnevale, N., Rozsa, B., & Zecevic, D. (2015). Electrical behaviour of dendritic spines as revealed by voltage imaging. *Nature Communications* 2015 6:1, 6(1), 1–12. <https://doi.org/10.1038/ncomms9436>
- Porterfield, V., & Porterfield, V. (2020). Neural Progenitor Cell Derivation Methodologies for Drug Discovery applications. *Assay and Drug Development Technologies*, 18(2), 89–95. <https://doi.org/10.1089/adt.2019.921>
- Purves, D., Augustine, G. J., Fitzpatrick, D., Hall, W., LaMantia, A.-S., & White, L. (2019). *Neurosciences, 6th Edition*.
- Quicke, P., Song, C., McKimm, E. J., Milosevic, M. M., Howe, C. L., Neil, M., Schultz, S. R., Antic, S. D., Foust, A. J., & Knöpfel, T. (2019). Single-neuron level one-photon voltage imaging with sparsely targeted genetically encoded voltage indicators. *Frontiers in Cellular Neuroscience*, 13, 39. <https://doi.org/10.3389/fncel.2019.00039>
- Ramesh, R., & Chaudhari, P. (2021). Model Zoo: A Growing "Brain" That Learns Continually. <https://doi.org/10.48550/arxiv.2106.03027>
- Rickgauer, J. P., Deisseroth, K., & Tank, D. W. (2014). Simultaneous cellular-resolution optical perturbation and imaging of place cell firing fields. *Nature Neuroscience* 2014 17:12, 17(12), 1816–1824. <https://doi.org/10.1038/nn.3866>

- Ronzitti, E., Ventalon, C., Canepari, M., Forget, B. C., Papagiakoumou, E., & Emiliani, V. (2017). Recent advances in patterned photostimulation for optogenetics. *Journal of Optics*, 19(11), 113001. <https://doi.org/10.1088/2040-8986/AA8299>
- Sage, D., & Unser, M. (2003). Teaching Image-Processing Programming in Java. *IEEE Signal Processing Magazine*, 20(6), 43–52. <https://doi.org/10.1109/MSP.2003.1253553>
- Schneider, C. A., Rasband, W. S., & Eliceiri, K. W. (2012). NIH Image to ImageJ: 25 years of image analysis. *Nature Methods* 2012 9:7, 9(7), 671–675. <https://doi.org/10.1038/nmeth.2089>
- Shen, S. P., Tseng, H. A., Hansen, K. R., Wu, R., Han, X., Gritton, H. J., & Si, J. (2018). Automatic Cell Segmentation by Adaptive Thresholding (ACSAT) for Large-Scale Calcium Imaging Datasets. *eNeuro*, 5(5), 56–74. <https://doi.org/10.1523/ENEURO.0056-18.2018>
- Sidhaye, J., & Knoblich, J. A. (2020). Brain organoids: an ensemble of bioassays to investigate human neurodevelopment and disease. *Cell Death & Differentiation* 2020 28:1, 28(1), 52–67. <https://doi.org/10.1038/s41418-020-0566-4>
- Sonka, M., Hlavac, V., & Boyle, R. (1993). *Image Processing, Analysis and Machine Vision*. Springer US. <https://doi.org/10.1007/978-1-4899-3216-7>
- Stirling, D. R., Swain-Bowden, M. J., Lucas, A. M., Carpenter, A. E., Cimini, B. A., & Goodman, A. (2021). CellProfiler 4: improvements in speed, utility and usability. *BMC Bioinformatics*, 22(1), 1–11. <https://doi.org/10.1186/s12859-021-04344-9>
- Stringer, C., Michaelos, M., & Pachitariu, M. (2020). Cellpose: a generalist algorithm for cellular segmentation. *bioRxiv*, 2020.02.02.931238. <https://doi.org/10.1101/2020.02.02.931238>
- Stringer, C., & Pachitariu, M. (2022). Cellpose 2.0: how to train your own model. *bioRxiv*, 2022.04.01.486764. <https://doi.org/10.1101/2022.04.01.486764>
- Tropepe, V., Hitoshi, S., Sirard, C., Mak, T. W., Rossant, J., & Van Der Kooy, D. (2001). Direct Neural Fate Specification from Embryonic Stem Cells: A Primitive Mammalian Neural Stem Cell Stage Acquired through a Default Mechanism. *Neuron*, 30(1), 65–78. [https://doi.org/10.1016/S0896-6273\(01\)00263-X](https://doi.org/10.1016/S0896-6273(01)00263-X)
- Winter, M., Wait, E., Roysam, B., Goderie, S. K., Ali, R. A. N., Kokovay, E., Temple, S., & Cohen, A. R. (2011). Vertebrate Neural Stem Cell Segmentation, Tracking and Lineaging with Validation and Editing. *Nature Protocols*, 6(12), 1942. <https://doi.org/10.1038/NPROT.2011.422>
- Winter, M. R., Liu, M., Monteleone, D., Melunis, J., Hershberg, U., Goderie, S. K., Temple, S., & Cohen, A. R. (2015). Computational Image Analysis Reveals Intrinsic Multigenerational Differences between Anterior and Posterior Cerebral Cortex Neural Progenitor Cells. *Stem Cell Reports*, 5(4), 609–620. <https://doi.org/10.1016/J.STEMCR.2015.08.002>
- Wu, Q., Merchant, F. A., & Castleman, K. R. (2008). *Microscope Image Processing*. Academic Press. <https://doi.org/10.1016/B978-0-12-372578-3.X0001-3>
- Zhuang, E., Qi, Z., Duan, K., Xi, D., Zhu, Y., Zhu, H., Xiong, H., & He, Q. (2019). A Comprehensive Survey on Transfer Learning. *Proceedings of the IEEE*, 109(1), 43–76. <https://doi.org/10.48550/arxiv.1911.02685>

APPENDIX 1. IOU AND F-SCORE MEASUREMENTS

Image	# of ROIs	Avg ROI size	T	S	TP	IoU	F-score
img1	1	50764	50764	45128	44510	0.866	0.928
img2	1	7205	7205	6956	6845	0.936	0.967
img3	1	4647	4647	5083	4512	0.865	0.927
img4	2	4754	9508	7781	7717	0.806	0.893
img5	1	14326	14326	15280	13828	0.8761	0.934
img6	2	8436	16872	16982	16167	0.914	0.955
img7	3	11920	35760	35081	29997	0.734	0.847
img8	8	3444.5	27556	23754	22416	0.776	0.874
img9	9	3574.444	32170	29754	27929	0.822	0.902
img10	7	5600.429	39203	34793	31705	0.750	0.857

Table 1: Segmentation accuracy measurements for the Fluorescence model. T - true object size, S - segmented object size, TP - true positives, area in pixels. IoU and F-score values are rounded up to 3 digits.

Image	# ROIs	Avg ROI size	T	S	TP	IoU	F-score
img1	29	2360.670	68460	65672	60822	0.829	0.907
img2	11	1947	21417	19751	17681	0.753	0.859
img3	14	1709.714286	23936	24220	21721	0.822	0.902
img4	33	1440.910	47550	46819	42114	0.806	0.893
img5	41	1236.512	50697	49066	42947	0.756	0.861
img6	36	1003.417	36123	33872	29584	0.732	0.845
img7	82	1190.963	97659	93602	84677	0.794	0.885
img8	24	1069.375	25665	22345	20226	0.728	0.843
img9	67	1039.448	69643	65224	59709	0.794	0.885
img10	55	1159.091	63750	57869	51814	0.742	0.852

Table 2: Segmentation accuracy measurements for the Phase-Contrast model. T - true object size, S - segmented object size, TP - true positives, area in pixels. IoU and F-score values are rounded up to 3 digits.

Microscope Setup Manual

0. Safety first! Close the door and use the interlock.

Hardware:

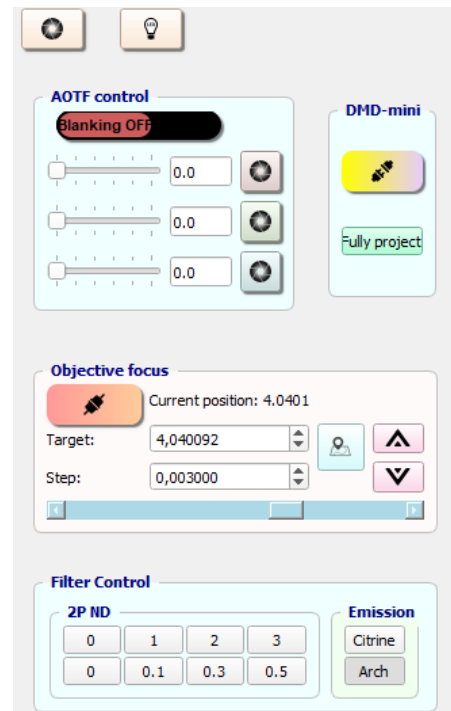
1. Switch on the blue and red lasers.
2. Check the power supply for AOTF - plug it in above the table.
3. Laser beam diameter can be adjusted with a variable telescope.
4. Remove protective cover from the objective.
5. Place a sample stage (the yellow cable should be on the top-left) by sliding it from left to right.
6. Tighten the clamps with a screwdriver if needed.
7. Add a droplet of MilliQ on the objective.
8. Check if the chiller cable is plugged in under the table.
9. Switch on the camera.

Software:

10. Login to the computer.
11. Use Hokawo software to control the camera. We need three tabs:
 1. ORCA Flash 4: control exposure time, start with 10 ms.
 2. Image format: set ~160-180 px vertically to reach 1000 fps acquisition rate; check the box “symmetric from the centre line.”
 3. Extern timing: the camera has its own clock. Switch to intern to control exposure time.
 4. The live imaging button is on the top panel.
12. Start the Spyder environment and run the first open tab.
 1. DMD: connect.
 2. AOTF: Blanking ON, then adjust lasers of needed wavelength.
 3. Objective focus: connect (it will take around 30 seconds).
 4. Filter control: Citrine/Arch; reset filters with the button if needed.
 5. To find cells, turn on the LED (lightbulb button).
 6. To change focus, use the slider bar, then buttons for fine-tuning.

Finishing work:

13. Disconnect the objective, turn off AOTF and stop DMD projection via the software.
14. Close the application and log out.
15. Remove a sample from the stage, then remove the stage itself.
16. Wipe the objective from MilliQ and place a protective cover.
17. Turn off and plug off pieces of hardware.



DMD Projection Manual

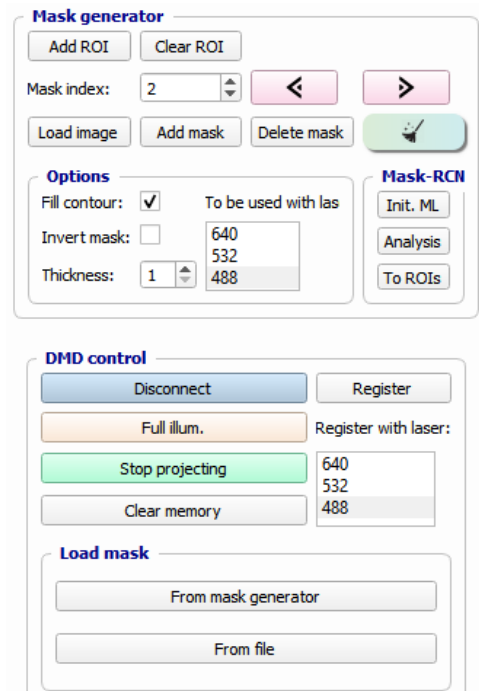
0. Safety first! Close the door and use the interlock.
1. Start with the “Microscope Setup” manual.
2. Go to the tab “DMD coordinates” in the Spyder environment.
3. Widget “Mask generator” allows to draw a mask manually, create a mask using automatic segmentation, or load an already generated mask.

To draw a mask manually:

- 3.1. Capture an image of the desired field of view using Hokawo software.
- 3.2. Load an image to the mask generator.
- 3.2. To draw, hover the cursor over the cell of interest and press the space bar, draw a contour, and then press the space bar again once finished.
- 3.3. **Important:** check the box “full contour” if it is necessary to do the projection on the entire cell; otherwise, DMD will project only a cell contour.
- 3.4. To create another mask (e.g., for fast switching experiments), do the following: change the mask index → click “Clear ROI” → draw a new mask → “Add mask”.
- 3.5. Indicate at the side menu with which laser wavelength defined mask should be used.

To use automatic segmentation:

- 3.6. Use the tab “Mask RCNN”. The algorithm will automatically segment cells and highlight them with different colors.
 - 3.7. Click on the cells of interest to create a mask.
4. Use the “Load mask” widget to load a mask from either a mask generator or an already existing file.
 5. Connect DMD via widget “DMD control” and press the button “Start projection”.
 6. Follow the manual “Fast Switching Recording” if you want to project different masks with different wavelengths.



Fast Switching Recording Manual

0. Safety first! Close the door and use the interlock.
1. Start with the “Microscope Setup” and “DMD Projection” manuals.
2. Once DMD masks are loaded, proceed to the widget “Settings” in the “DMD coordinates” tab. Use settings on the image below, filling in the desired DMD switching frequency and clicking the button “Fill in illu. time for Hz” to adjust illumination time automatically.

3. Go to the “Waveforms” tab (see the screenshot below). Set the directory where you want to save configured waveforms.
4. Use 488AO as a reference waveform in the “General settings” widget.
5. Setting up Analog signals in the “Block” tab, parameters of interest:

Signal	Frequency (Hz)	Offset (ms)	Duration (ms)	Duty cycle (%)
488AO	half of DMD’s	0	desired duration of the recording	50
640AO	half of DMD’s	half-period*		50


Starting amplitude may vary, but usually, it is 5V.


* If the frequency is 500 Hz, one period lasts 2ms. Thus, minding a 50% duty cycle, the offset for a 640nm laser must be 1 ms. The first mask will be projected with blue illumination, and the second – with red.

6. Setting up Digital signals:

Signal	Frequency (Hz)	Offset (ms)	Duration (ms)	Duty cycle (%)
DMD trigger	as in the “Coordinates” tab	0	desired duration of the recording	50
Camera trigger	**	0		50
Blankingall	as DMD’s	0		100

** typically, the camera trigger rate is half of the DMD trigger rate, but it might depend on a particular experiment.

7. “Execution” widget – check the box “Save waveforms” so that in case of an identical experiment you do not need to configure waveforms again, choose Arch emission filter to record cells with red illumination.
8. Press the button “Configure”: 
9. Go to Hokawo software and switch the camera to extern trigger – it will wait for the trigger from the I/O device (hardware synchronization).

10. Hokawo “Stream” tab: set the directory to save the recording → indicate buffer size, it must be larger than the number of frames → “Apply” → “Start streaming”.
11. Go back to the “Waveforms” tab, press “Execute”: 
12. The recording will be saved in the configured path as a .tif file.

Waveforms

General settings

Reference waveform

- galvos
- galvos_contour
- 640AO
- 532AO
- 488AO

Recording

---PMT---

---Vp---

---Ip---

Sampling rate: 500000

Master clock: DAQ

Load waveforms

Execution

Save waveforms

Progress:

Emission filter

Arch

GFP/Citrine

Execute

Canvas

Analog signals

640AO + ×

Block: Ramp Galvo Photocycle

Frequency /s: Duration (ms, 1 cycle): Duty cycle (%):

Offset (ms): Steps in duration: Gap between cycles (samples):

Starting amplitude (V): Change per step (V):

Baseline (V): Number of cycles:

Digital signals

cameratrigger + ×

Block:

Frequency /s: Duration (ms): DC (%):

Offset (ms): Repeat: Gap between repeat (samples):

Waveform plot

